Appl. Phys. B 84, 75–82 (2006)
DOI: 10.1007/s00340-006-2201-6

Applied Physics B
Lasers and Optics

B.M.A. RAHMAN✉
A.K.M.S. KABIR
M. RAJARAJAN
K.T.V. GRATTAN
V. RAKOCEVIC

Birefringence study of photonic crystal fibers by using the full-vectorial finite element method

School of Engineering and Mathematical Sciences, City University, Northampton Square, London EC1V 0HB, UK

Received: 19 January 2006
Published online: 8 April 2006 •

ABSTRACT Modal solutions of photonic crystal fibers with equal and unequal circular air holes in a hexagonal matrix are presented, by using a rigorous full-vectorial finite element-based approach. The effective indices, mode field profiles, spot-sizes, modal hybridness, modal birefringence and group velocity dispersion values have been determined and presented. The effects of the pitch-distance, hole diameter, structural asymmetry, air hole arrangement and the operating wavelength on the modal birefringence are also reported. It is shown that a significant value of birefringence can be achieved by using only circular air holes, which would be easy to fabricate, and by operating it close to its modal cutoff.

PACS 42.81.Qb; 42.81.Gs; 42.25.Bs; 31.15.Pf

1 Introduction

Photonic crystal fiber (PCF) (which is also known as 'holey' fiber), is a micro-structured fiber [1], where arrays of holes run along the waveguide length of the fiber, which have more controllable fabrication parameters than standard single mode fiber (SMF). Increasing interest is being shown in such PCFs for a range of applications in optical communications, sensing and signal processing. The optical properties of a SMF are mostly controlled by two key parameters: the radius and the index difference between the core and the cladding. An SMF can be designed by balancing these two parameters for different applications, for example in conventional low-loss telecommunications grade SMFs or in specialized fibers such as doped fibers, offering a smaller spot-size. However, the potential for adjustment of the group velocity dispersion (GVD) properties of these silica fibers is severely limited. By contrast in a PCF, the numbers of holes, their sizes, shapes, orientations and placements, as well as the nature of the dielectric material, can provide additional degrees of freedom, which are not present in conventional SMF. A wide range of potential applications is anticipated, exploiting the ability to adjust the spot-size, for example to create a large spot-size for high power applications and a smaller spot-size for improved nonlinear interactions. The zero dispersion point can be shifted into the visible part of the spectrum [2] and the GVD properties can be tailored to facilitate Raman amplification, Brillouin lasers, second harmonic generation, four-wave mixing, and supercontinuum generation [3] at modest powers. The higher index contrast of the PCFs would enhance their polarization maintaining properties, which are useful for coherent optical communication and fiber optic sensor systems. In spite of the progress made in the fabrication of PCFs, including birefringent PCFs, so far their birefringent properties have not been thoroughly studied.

Conventional silica fiber with circularly symmetric homogeneous core cannot maintain the polarization state of the output field, due to bends, twists, stress and random irregularities along the length of the fibers. Modal birefringence in optical waveguides can reduce the polarization coupling, which can be achieved in different ways, including through the use of anisotropic materials. However, for a nominally isotropic silica fiber, the alternative approach is to create a spatial asymmetry in the index profile or shape profile. Due to small index contrast between the core and cladding, the form birefringence is also relatively small for noncircular core silica fibers, such as the elliptic core silica fibers. An attractive alternative approach had been used to change the isotropic material to anisotropic by introducing an asymmetric stress profile. This can be achieved by introducing stress-applying zones, with unequal thermal expansion coefficients and the resultant highly-birefringent (Hi-Bi) 'Panda' or 'Bow-tie' fiber have shown a birefringence value in the range of 5×10^{-4} [4, 5].

However, highly birefringent PCFs can be more easily realized, because the index contrast is higher than that of conventional fibers and the fabrication process permits the formation of the required asymmetric microstructure near the fiber core. The structural symmetry can be destroyed either by changing the air hole sizes near the core area [6–8], or by deforming the shape of the air holes [9, 10] or the core shape [11]. A numerical study by Steel and Osgood [9] indicated that using elliptical-shape air holes and operating very close to the modal cutoff, a significantly large birefringence could be obtained. It was also suggested that such highly elliptical air holes could be fabricated in the preform by modifying their nominal circular air holes by drilling to increase the asymmetry. It has been shown that using the 'stack-and-draw' fabrication process permits the formation of the asymmetry near the fiber core more easily with circular holes and the

✉ Fax: +44-20-7040-8568, E-mail: b.m.a.rahman@city.ac.uk

resulting birefringence value is of the order of 10^{-3} [6, 11], which is significantly larger than that of the Panda or Bow-tie silica fibers.

The large birefringence that may be achieved is very promising for PCF devices such as lasers [12], fiber loops for gyroscopes, rocking filters [13], and two-mode strain sensors [14]. In this study, the interplay between the various fabrication parameters at a given wavelength on the modal solutions of the quasi-TE and TM modes is discussed. In this work, the largest value of the modal birefringence is found by adjusting the pitch length and the normalized hole diameter for a PCF with circular but unequal air holes. This design is easy to fabricate by using the stack-and-draw technique.

2 Theory

To date, most of the research into these fibers has had a strong experimental basis [1], which has recently been complemented by various modal solution approaches to their characterization, but mostly using scalar formulations or being limited to specific types of structures. One of the simplest methods used is the effective index method [2], which approximates the PCF to a step index fiber with the cladding index equal to the average or weighted average of the PCF in the cladding region. Although it can provide some insight into PCF operation, this reduced model is unable to accurately predict the fiber modal properties such as dispersion or birefringence, which depend critically on the arrangement and size of the air holes.

Several numerical approaches have been considered by using mode decomposition techniques, based on the expansion of the modal field. The plane wave method (PWM) [15] utilizes sinusoidal basis functions, which can be used for any refractive index profile if enough basis functions are used, and thus a versatile, but not so efficient approach, as it does not take advantage of the localization of the guided modes. In the full-vectorial technique described by Ferrando et al. [16] the modal fields and the refractive index profile are decomposed into plane wave components, finally reducing the wave equation to an eigenvalue problem. Mogilevsov et al. [17] considered an alternative scalar approach by using a more selective localized Hermite–Gaussian orthogonal basis function (LFM) expansion to represent the transverse magnetic field. Expanding the fields in localized Hermite–Gaussian functions [18, 19] can be more efficient, however these functions have an adjustable width parameter, the value of which is not a priori known, and would be different for different PCFs or even for different modes in a given fiber. Subsequently, Monro et al. [20] introduced a full-vectorial model for PCFs with a perfect hexagonal arrangement of holes. Several groups have used the multipole method (MM) [21], in which the vectorial fields are expanded about each circular hole by using Bessel and Hankel functions, but unfortunately this is restricted to circular shaped holes only. Recently Zhi et al. [22] have considered the supercell overlapping method by combining the PWM and the LFM to study square and triangular lattice PCFs. However, in these field expansion methods, when the noncircular air-holes are approximated by circular holes, as in the plane wave method [6] or in the multipole method [23], the important polarization dependent properties would be lost. Most of the expansion methods also require periodic boundary conditions, which do not allow any calculation of the confinement losses due to the energy leakage between and through the holes, whereas these leaky modes are characteristic of all real PCFs. The periodicity required is also somehow restrictive for PCFs, which do not need to be periodic, and in reality they never are perfectly periodic.

Amongst the more general numerical methods available, the finite difference [24] and the boundary element method [10] based modal solution approaches have also been considered. The beam propagation method [25] can be used to simulate the propagation of the initial field along a PCF, and more recently the imaginary distance BPM has been used [26–28] to extract a limited number of individual modes, but the BPM approach is computationally more intensive, since it needs to consider a fully three-dimensional structure.

To obtain accurate modal solutions of PCFs, first of all it is necessary to accurately represent its two-dimensional complex cross-section profiles. The modal solution approach, based on the powerful finite-element method (FEM) [29] is more flexible, and can be used to represent any arbitrary cross-section more accurately and has been widely used to find the modal solutions of a wide range of optical waveguides. In the finite element method, by using a larger number of triangular elements, which may have different shapes and sizes, any complex optical waveguide cross-section can be accurately represented. The flexibility of the FEM to represent a cross-section of a holey fiber, with arbitrary hole sizes, shape, orientation, placements and materials, makes it a powerful approach where many other simpler and semi-analytical methods are unsatisfactory. Recently Koshiba and Saitoh [30], Brechet et al. [31], Peyrilloux et al. [32], and Cucinotta et al. [33] have considered the full vectorial FEM, which has been shown to be the most suitable method to study complex modal characteristics of such PCFs.

In the finite element or finite difference method, the variational formulation can be based on the fully vectorial or simpler scalar formulation approach. The optical modes in a high-index contrast PCF with two-dimensional optical confinement are also hybrid in nature, with all the six components of the $\boldsymbol{E}$ and $\boldsymbol{H}$ fields being present. To accurately characterize such fibers, a full-vectorial approach is essential and such a $\boldsymbol{H}$-field based full-vectorial approach is extended to obtain the modal solutions of PCFs. The complete $\boldsymbol{H}$-field formulation with the augmented penalty parameter is given as [29]:

$$\omega^2 = \frac{\int (\nabla \times H)^* \hat{\varepsilon}^{-1} (\nabla \times H)\, \mathrm{d}\Omega + \left(\frac{\alpha}{\varepsilon_0}\right) (\nabla \cdot H)^* \cdot (\nabla \cdot H)\, \mathrm{d}\Omega}{\int H^* \hat{\mu} H\, \mathrm{d}\Omega} \tag{1}$$

Here $\boldsymbol{H}$ is the full-vectorial magnetic field, ε and μ are the permittivity and permeability, respectively of the waveguide, ε_0 is the permittivity of free space, ω^2 is the eigenvalue, where ω is the angular frequency of the wave and α is a dimensionless parameter used to impose the divergence-free condition of the magnetic field in a least squares sense. In this formulation both the ε and μ can be arbitrary tensors with possible off-diagonal coefficients, suitable to characterize electro-optic, acousto-optic and elasto-optic devices. The isotropic silica material in PCF can become anisotropic under

thermal stress or applied force, or if the air holes are filled up with an anisotropic fluid, such as in device applications using a liquid crystal. Similarly, the above formulation can also consider the lossy surface plasmon mode [34] in metals, where the permittivity is negative, and an incorporation of such metal nano-tubes in future PCFs can also be considered. A similar formulation has also been considered to find the lightwave propagation [35] in erbium doped active PCF devices with modal gain. Modal solutions for the fundamental and higher order quasi-TE and quasi-TM modes have been obtained in this work. The modal field profiles, the variation of their spot-sizes, the modal hybridism, the modal birefringence, and the GVD properties have been calculated for these fibers. The use of infinite elements extended the orthodox computational domain of the open-type optical waveguides. The infinite elements can accurately represent the exponentially decaying optical field outside the core region. This approach can yield accurate solutions for the optical modes. Although, if perfectly matched layers (PML) are used, another important parameter, the leakage loss can be obtained but in this case the eigenvalue equation would be complex and the computational time would be at least double. The existing two-fold symmetry has been exploited to reduce the computational cost and also to achieve adequate mesh refinement in the core region.

3 Results

For a regular array of holes of equal size, the hole diameter is taken as d with Λ as the pitch length. A missing hole at the center can guide the light, as does the core of a typical optical waveguide. First, the effect of the hole diameter, d, on the modal properties is investigated and the variations of the effective index and the spot-size for the fundamental quasi-TE (H_{11}^y) mode with the normalized d/Λ dimension are shown in Fig. 1. Initially the pitch length, Λ (the center-to-center spacing between two nearest air holes) has been kept fixed at 2.2 μm. In this case the refractive index of the silica is taken as 1.46232 at the operating wavelength of 0.5 μm. With the pitch, Λ, fixed at 2.2 μm, and as the hole diameter d, is increased, the equivalent index of the air hole cladding region is reduced, which increases the index contrast between the effective cladding and the solid silica core. Although the reduced cladding index reduces the modal effective indices, the increased index contrast makes the mode better confined. It should be noted that, in the present approach, all the air holes, including their sizes and positions are exactly represented. In this figure, it can also be observed that as the hole diameter is increased, the spot-size (σ) is reduced. This is because the enlargement of the holes restricts the escape of the modal field from the core area. In this case the spot-size is defined as the area where the field intensity is greater than $1/e$ of the maximum field intensity (power intensity $1/e^2$). More than 28 000 first order irregular size triangular elements have been used to represent only one-fourth of the PCF cross-section and a typical computational time on a 2 GHz PC is less than one minute.

The dominant H_y field profiles of the fundamental quasi-TE (H_{11}^y) mode for $d/\Lambda = 0.3$ and 0.7 at the operating wavelength of 0.5 μm are shown in Fig. 2a and b, respectively. It can be clearly seen that for a lower value of the air hole diameter, the field extends into the silica bridging area (in-between the air holes). However, for the larger air holes with a narrow bridging area, the field is more confined in the core, as they are restricted from the low-index air regions. The effect of the hole diameter on the spot-size is clearly visible, and its variation is shown in Fig. 1.

The FEM approach is a very versatile method and its strength has been the easy manner of changing the position and size of any of the air holes, as they are required. By changing the shape of the holes or the size of some selected air holes, the structural symmetry can be avoided and this yields another important modal property, the modal birefringence. In the hexagonal arrangements, air holes are placed in concentric rings around the core. Since, the influence of the air holes in the first ring would be dominant, to break the structural symmetry, modification of the air hole dimensions in this ring would be more effective. The asymmetry arrangement considered here is similar to that found in [36], where the diameters (d_2) of the four air holes in the first ring are different from that of the other diameters (d). The inset in Fig. 3 shows only a single air hole in a quarter of the cross-section used in the numerical simulations. Such an asymmetric PCF would be able to maintain a specific input polarization state, and the corresponding modal birefringence is expected to be high. In this case, initially the pitch, Λ, is taken as 2.2 μm with the operating wavelength as 0.5 μm. The diameter of asymmetric air hole (d_2) is varied and the diameters of all the other holes are kept fixed at 1.1 μm ($d/\Lambda = 0.5$). The variations of the effective indices for the fundamental quasi-TE (H_{11}^y) and quasi-TM

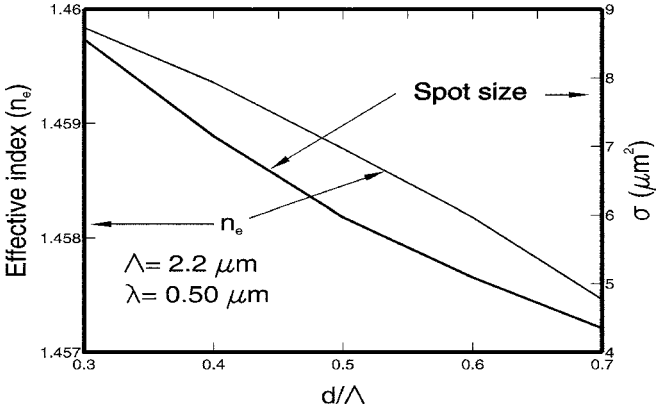

FIGURE 1 Variations of the effective index and spot-size with the normalized hole diameter d/Λ

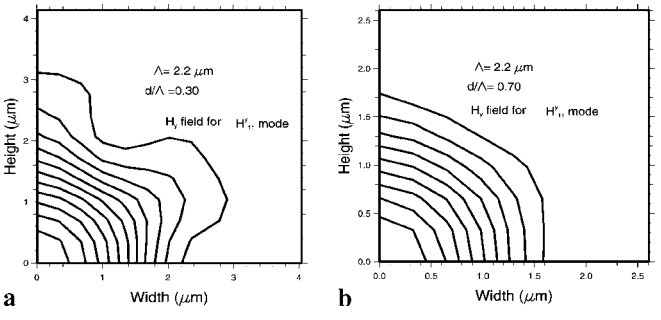

FIGURE 2 Dominant H_y field profile of the fundamental quasi-TE mode for (**a**) $d/\Lambda = 0.3$ and (**b**) $d/\Lambda = 0.7$

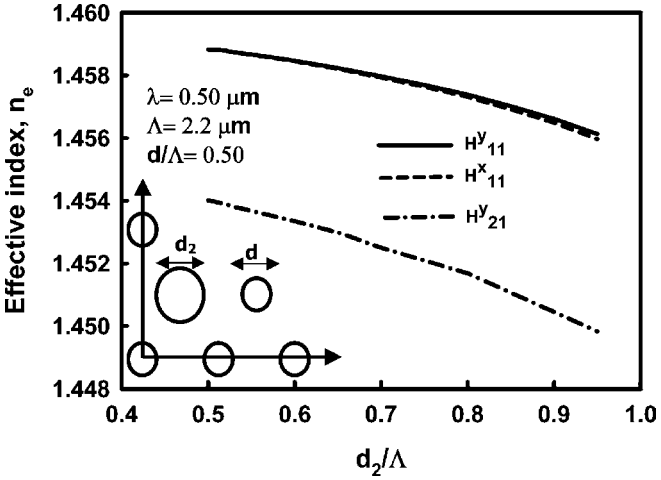

FIGURE 3 Variations of the modal indices with the normalized diameter, d_2/Λ

(H_{11}^x) and the second quasi-TE (H_{21}^y) modes with the normalized asymmetry (d_2/Λ) are shown in Fig. 3. It can be observed that as the diameter of the air hole, d_2, is increased, the effective index values decrease. This is due to the fact that with the increased air hole size, the equivalent cladding index is reduced. It can be clearly observed that as d_2 is increased, the modal index difference between the two fundamental TE and TM polarized modes increases. This arises because the increased d_2 diameter makes the PCF structure more asymmetric. An increased d_2 value makes the height of the effective core smaller than that of the width and as a consequence the effective index of the quasi-TE mode is higher than that of the quasi-TM mode. For comparison, the effective index variation of the H_{21}^y mode is also shown in this figure. It was observed, but not shown here, that the spot-size reduces as the d_2 diameter is increased as the increased air hole diameter restricts the optical field in that air hole region.

The variations of the modal birefringence, B, and the beat length, L_B, are shown in Fig. 4 for the case where the operating wavelength is 0.5 μm. In this case the modal birefringence is defined as:

$$B = n_y - n_x \tag{2}$$

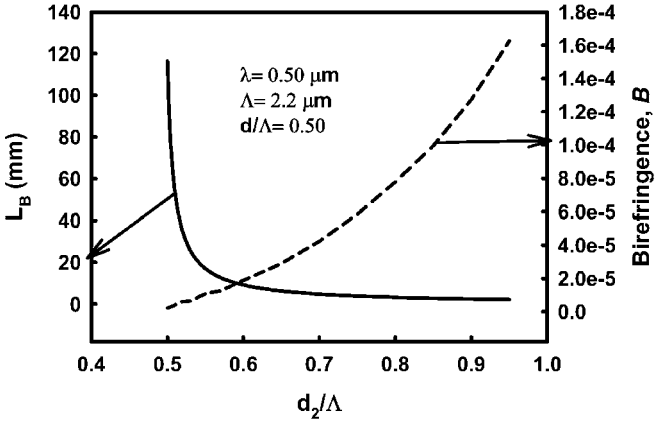

FIGURE 4 Variations of the beat length and modal birefringence with the normalized d_2/Λ for $\Lambda = 2.2$ μm

where n_y and n_x are the effective indices of the fundamental H_{11}^y and H_{11}^x modes, respectively. The polarization beat length, L_B, is a measure of the birefringence and is defined as:

$$L_B = 2\pi/(\beta_y - \beta_x) = \lambda/B \tag{3}$$

where β_y and β_x are the propagation constants of the H_{11}^y and H_{11}^x modes, respectively. It can be clearly observed that the birefringence value increases as the d_2 value is increased, since the asymmetry of the PCF structure is also increased. In this case the maximum birefringence value of 1.6×10^{-4} is achieved, which is comparable to the birefringence of polarization maintaining Panda or Bow-tie type Hi-Bi fibers.

The group velocity dispersion (GVD) is one of the most important modal properties of an optical waveguide and this parameter, D, can be defined as:

$$D(\lambda) = -\frac{\lambda}{c}\frac{\partial^2 n_e}{\partial \lambda^2} \tag{4}$$

where n_e is the effective index of a given mode and c is the speed of light in the free-space.

Variations of the GVD with the operating wavelength for the quasi-TE (H_{11}^y) and quasi-TM (H_{11}^x) modes for the asymmetric structure with $d_2/\Lambda = 0.95$ are shown in Fig. 5 by a dashed line and a solid line, respectively. Chromatic dispersion of the silica has been taken into account by calculating the refractive index of silica through the Sellmeier equation [37]. For comparison, the GVD of a degenerate PCF with identical air holes, $d/\Lambda = d_2/\Lambda = 0.5$, is also shown in this figure by a dashed-dotted line. It can be observed that by controlling the diameters of the air holes, the range of anomalous dispersion, the maximum value of the GVD and its slopes, and the locations of the zero GVD value can be adjusted and similar adjustable GVD properties cannot be achieved in the design of a less flexible telecommunication grade SMF. The polarization dependence of the asymmetric PCF can be clearly observed and so various polarization dependent linear and nonlinear devices can be fabricated by using such birefringent PCFs.

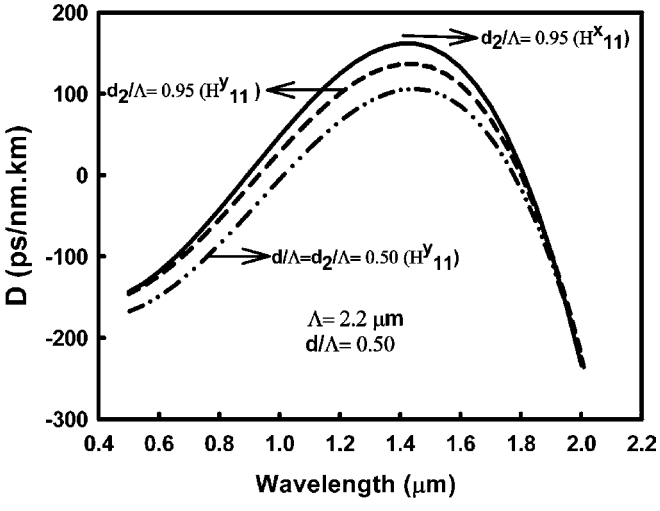

FIGURE 5 Variations of GVD with the operating wavelength

Besides the structural asymmetry, the birefringence value also depends on the modal confinement. For a fixed pitch length, $\Lambda = 2.2\,\mu$m, as the operating wavelength, λ, is increased, the modes become more weakly confined and the modal field extends further into the air hole regions. The variation of the modal birefringence, B, with the operating wavelength, λ, is shown in Fig. 6. In this case the d/Λ value is kept constant at 0.5 and the asymmetric air holes with their normalized diameter $d_2/\Lambda = 0.95$. It can be observed that as the operating wavelength is increased to 2.0 μm, the birefringence increases significantly to a value of 0.0071 with the corresponding beat length, L_B, reduced to 281 μm. This result agrees well with the numerically simulated result reported by Saitoh and Koshiba [36] of $B = 0.00327$ at a wavelength of 1.45 μm.

It can be observed that the birefringence value increases rapidly with the operating wavelength. Earlier it has been reported that the birefringence and the operating wavelength could be related by

$$B \alpha \lambda^{\kappa} . \tag{5}$$

To obtain the κ dependence, a log-log plot is also shown as an inset in Fig. 6. The near straight line relationship demonstrates a fixed value of κ, and from the slope of this line, the value of κ has been calculated as 1.6. It should be noted that the κ value depends on the specific design parameters of the PCF and values of 1.38 [6] and 2.7 [8] have been reported.

The pitch length, Λ, the operating wavelength, λ, and the normalized hole diameter d/Λ, all play key roles in the modal properties and additionally the asymmetry d_2/Λ for the birefringence properties. For a fixed operating wavelength, the pitch length, Λ, can be used as the key controlling parameter. Variations of the effective indices of the fundamental quasi-TE (H_{11}^y) mode with the pitch length, Λ, are shown in Fig. 7 for two d/Λ values when the operating wavelength is 1.55 μm. In this case, when the waveguide dimension is reduced compared to the wavelength, the modal field is extended further into the cladding region. In both the cases, the modal effective indices reduce monotonically as the pitch length, Λ, is reduced. It can be observed that the effective index values are lower for PCFs with larger d/Λ values, since in these cases the equivalent cladding indices were also lower. It should also be noted that, for a larger d/Λ value the index contrast is higher, and the cutoff value of the pitch length, Λ, is also smaller, as is shown here.

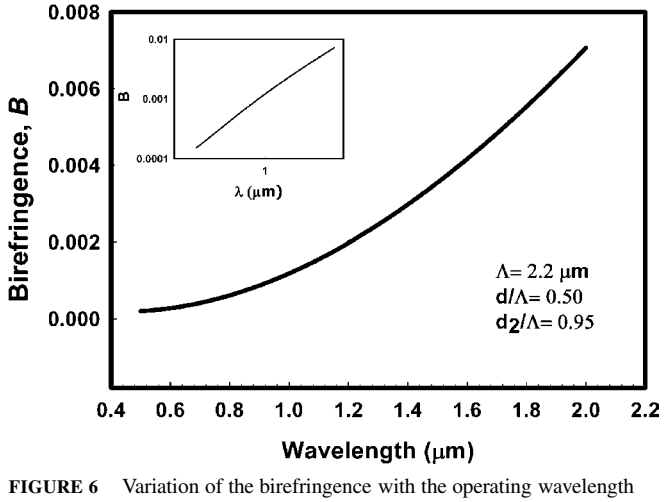

FIGURE 6 Variation of the birefringence with the operating wavelength

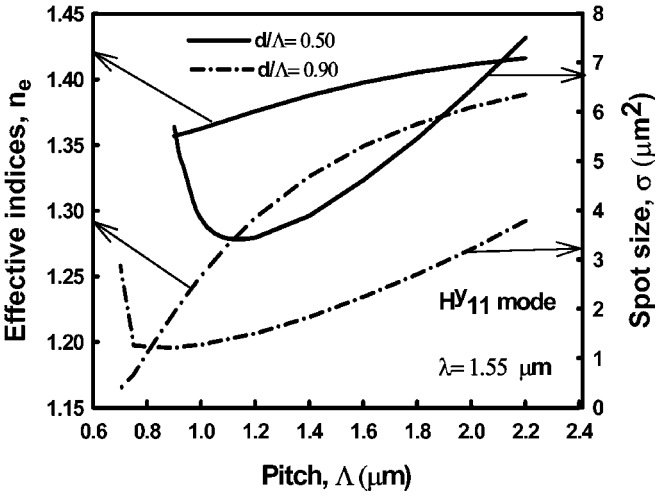

FIGURE 7 Variations of the effective indices and the spot-size with the pitch length, Λ

Variations of the spot-size with the pitch length, Λ, are also shown in Fig. 7. It can be noted that as the pitch length, Λ, is decreased, the waveguide dimension is reduced compared to the operating wavelength, the mode approaches its cutoff condition, the modal field expands and as a consequence the spot-size also increases, in a way similar to what was observed experimentally by Baggett et al. [38]. It should be noted that with a larger d/Λ value, the hole diameters are large, which restricts the mode in a narrower silica region and so the spot-size is smaller. The minimum spot-size value of 3.42 μm^2 can be achieved for a d/Λ value of 0.5, when $\Lambda = 1.14\,\mu$m at the operating wavelength of 1.55 μm. On the other hand if the d/Λ value is increased to 0.9, the minimum spot-size could be as low as 1.2 μm^2 at $\Lambda = 0.90\,\mu$m, one of the lowest reported so far. For many nonlinear applications, the reduction of the spot-size is a key issue, where an example of this is the usage of sub-micron guides in supercontinuum generation [39, 40]. It can be noted that for a larger d/Λ value, the cutoff condition approaches more rapidly due to the larger index contrast between the silica core and the effective cladding.

The variations of the dominant H_y fields for the quasi-TE (H_{11}^y) mode along the x-axis are shown in Fig. 8. In this case the horizontal distance is normalized (x/Λ), so that for all the Λ values, the air holes are located at the same normalized position. It can be observed that the field decays away from the PCF core and reduces substantially in the air hole region and increases locally beyond the air holes. It should be noted that, for $\Lambda = 0.95\,\mu$m (the mode being close to its cutoff) the field magnitude in the cladding region is significantly large. Although, in this figure for $\Lambda = 2.2\,\mu$m, the normalized field spread appears to be the smallest, but in fact the spot-size is much larger as the pitch length is much longer.

For a PCF with a regular hexagonal hole arrangement of a fixed diameter, a six-fold or 60 degree rotational symme-

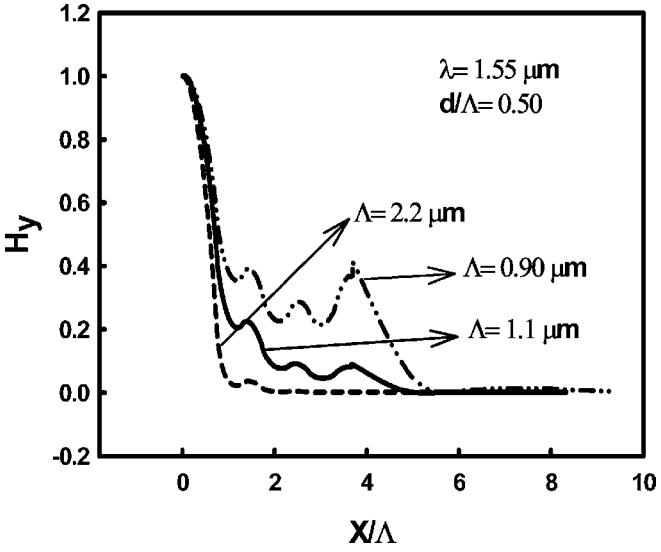

FIGURE 8 Variations of the modal fields in the normalized x direction

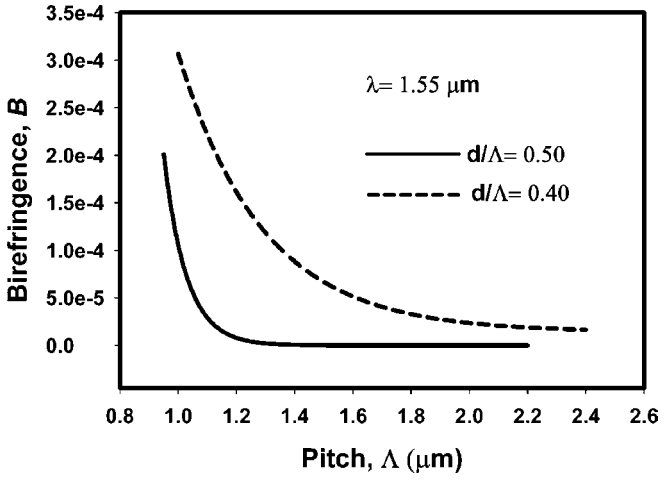

FIGURE 9 Variations of the birefringence with the pitch length, Λ

try exists, which makes the modes degenerate. There will be degenerate modes with the polarization directions rotated 60 degrees from each other. However, strictly speaking the vertically polarized TE and horizontally polarized TM modes would not be degenerate as the required 90 degrees rotational symmetry does not exist. Despite very good hexagonal symmetry in the fabricated PCFs, the existence of high birefringence in such PCFs has been measured by several groups [32, 41–43] but this has often been attributed to possible internal stress or to slight asymmetry, due to variations in the positioning and the diameters of the air holes. In several numerical studies, the structural representations have been systematically refined by using the finite element method [32, 44] and the plane wave method [45]. In all of these cases, a small residual birefringence remained, again attributed to the intrinsic calculation error of the computational approach. However, from these reports [32, 45] it could be clearly observed that this residual birefringence value is larger for smaller Λ/λ values.

Variations of the birefringence with the pitch length, Λ, for a PCF with six-fold symmetry for two different d/Λ ratios are shown in Fig. 9. In this case the operating wavelength is fixed as 1.55 μm. For a PCF with a larger Λ/λ value, the birefringence is very small but it can also be observed that as the pitch length, Λ, is reduced, the birefringence value is increased due to the larger modal field values in the air/silica cladding region. It should be noted that for some special cases the birefringence could be zero but in general this is not true for all the regular PCF structures with a six-fold symmetry, and more particularly when operating close to their cutoff points. It can be noted that for higher d/Λ values, the birefringence changes rapidly with Λ as their corresponding cutoff condition also approaches rapidly. One important validation of this work is the existence of the modal birefringence for PCFs with six-fold rotational symmetry.

Modes in optical waveguides with two-dimensional confinement are not truly TE or TM, but hybrid in nature. For quasi-TE (H^y_{mn}) modes, the H_y field component is dominant: however the non-dominant field, H_x is not zero. The modal hybridness is an important parameter in the design and operation of many optical systems, particularly to identify polarization-dependent performance, the modal losses, and possible polarization conversion. The modal hybridness can be defined as the ratio of the maximum values of the non-dominant to the dominant field components values. For the quasi-TE (H^y_{mn}) modes, the hybridness is defined as the ratio of the non-dominant H_x field to the dominant H_y field. Variations of the modal hybridness with the pitch length, Λ, for the fundamental H^y_{11} mode are shown in Fig. 10 for $d/\Lambda = 0.4$, 0.5 and 0.6, by dashed-dotted, dashed and solid lines, respectively. The modal hybridness increases as Λ is reduced and reaches a maximum value when the spot-size is near to its minimum value. It can also be noted that for a higher d/Λ value, the maximum hybridness value is also higher due to the associated higher index contrast. It was also observed that for the quasi-TM modes, the patterns of the hybridness variations were similar.

It is expected that a lower pitch length, Λ, would produce a higher birefringence for a given structural asymmetry. To achieve a higher birefringence value, a smaller pitch length of $\Lambda = 1.1$ μm was considered. It was mentioned earlier, that the diameters of either two air holes [46] or four air holes [36] in

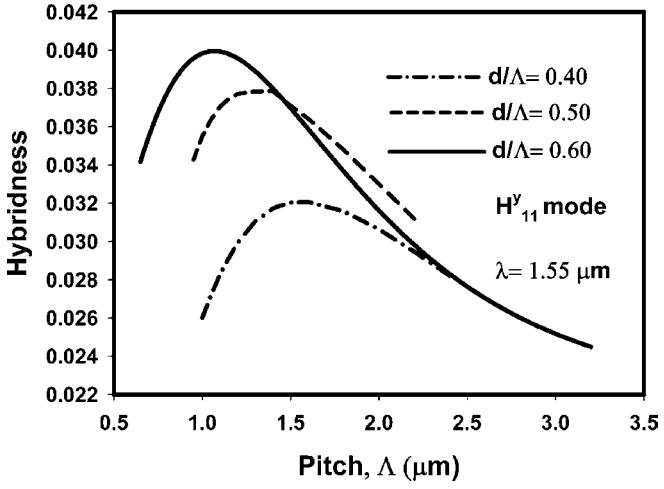

FIGURE 10 Variations of the modal hybridness with the pitch length, Λ

the first ring could be changed to break the rotational symmetry. The variations of the birefringence (B) with the normalized air hole diameter, are shown in Fig. 11 for both the cases, when $\Lambda = 1.1$ μm and the operating wavelength $\lambda = 1.55$ μm. Hole arrangements are also shown in this figure as an inset. It can be clearly observed that for four-hole arrangements, shown by the dashed line as $d_2 > d$, the birefringence is positive and similarly when $d_2 < d$, the birefringence values are negative. It can be noted that for higher d_2/Λ values, the effective index value of the quasi-TE mode is higher than that of the quasi-TM mode, as in this case the equivalent core width is larger than its height. Similarly, when the d_2/Λ value is lower, the effective index value of the quasi-TM mode is higher as in this case the equivalent width is smaller than its equivalent height. This birefringence value increases rapidly when d_2 is much larger than d, as both the TE and TM modes approach their cutoff values and their difference increases. It can be noted that in this case the maximum birefringence value is significantly higher, reaching a value of 0.0062, the highest at this wavelength for an asymmetric PCF using circular air holes. It should also be noted that the birefringence value of such a simple PCF with circular holes is significantly high, compared to the polarization maintaining Panda or Bow-tie fibers [5] and thus is useful for many practical applications in optical communications and sensing. When the d_2/Λ value is larger than 0.85, this particular PCF cannot guide the H_{11}^x mode and the PCF structure becomes a single polarization guide.

On the other hand, for the two-hole arrangement as shown by a solid line, when $d_1 < d$, the birefringence is positive as the effective width is larger than its height. However, when d_1 is much larger than d, although the birefringence is negative, this value does not increase significantly. In this case, since the equivalent cross section is only slightly reduced, the modal cutoff conditions of the two fundamental modes are not reached. It should be noted that the experimental results for similar air hole asymmetry and modal confinement (but with only two air holes [46] enlarged) yielded a much lower birefringence and a value of $B = 0.00258$ was reported [13], which agrees well with that reported in this work.

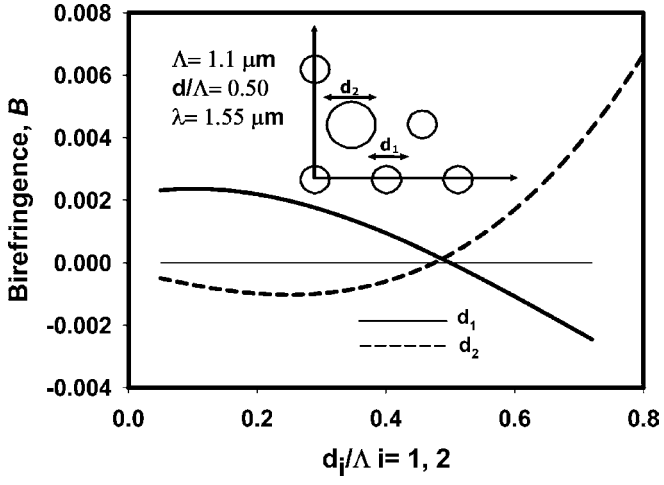

FIGURE 11 Variation of the birefringence with two different structural asymmetry values, d_i/Λ, $i = 1, 2$

4 Conclusions

Important design parameters, such as the effective indices, the modal field profile, the spot-sizes, the modal hybridness, and the GVD are determined and presented for PCFs with equal and unequal circular holes, by using a rigorous full-vectorial finite element-based approach. This is a versatile approach, which can be used to represent any arbitrary-shaped PCF with arbitrary hole shapes, sizes, orientations, materials and placement. The variations of the GVD, an important optical parameter, are shown and it appears to be possible to design a PCF with a specific GVD, or other optical properties, by adjusting the different fabrication parameters. It is clearly shown that, in a PCF with six-fold rotational symmetry, despite having degenerate modes, the horizontally and vertically polarized quasi-TE and TM modes are not degenerate and the modal birefringence can be increased by operating near their modal cutoff.

It is well known that the form birefringence of silica fiber is smaller due to the smaller index contrast and additional birefringence may be introduced using stress-applying parts, with different thermal expansion coefficients, as in the design of Panda type fibers. On the other hand, the form birefringence of a PCF can be significantly higher than that of the Panda fibers because of their higher air/silica index contrasts. So far, the highest value of the birefringence, $B = 0.0062$, for any PCF with circular air-holes is also reported. In Panda type fibers, due to thermal stress, both the ordinary and extraordinary indices changes, but their spatial variations are nonuniform [5] and their difference, although larger than the form birefringence of solid silica fiber, are smaller relatively than the form birefringence of asymmetric PCFs. Folkenberg et al. have designed a polarization maintaining [47] and a single polarization [48] PCF with the stress applying parts to increase the birefringence. Since the designs used identical air holes, with low form birefringence, the increased birefringence values due to the stress present were between 1×10^{-4} [46] and 3×10^{-4} [47], which is of a similar order to that in a Panda or Bow-tie silica fiber.

The air holes of a PCF can also be selectively filled up with other materials having different refractive index values, such as polymer [49], to create a structural asymmetry. Besides obtaining a moderate birefringence value, of the order of 10^{-3}, this parameter can also be tuned through temperature adjustment. When the refractive index change of the polymer, $\partial n/\partial T$, is taken as -4×10^{-4} /°C, this yields a birefringence change of the order of $\partial B/\partial T \sim 3 \times 10^{-6}$ /°C. It has also been shown that twisting or bending of the fibers also introduces additional birefringence. Under external force, a waveguide deforms and due to the elasto-optic effect both the profiles of the ordinary and extraordinary refractive indices change. However, these birefringence changes have been modest and Zhu and Brown [50] have reported a birefringence change of 10^{-4} , for an applied force of 1000 Nm.

Although the effects of stress applying zones, temperature changes, and applied pressure on the enhancement of the birefringence in such highly birefringent PCFs appear to have been limited, these physical parameters can however be used to tune the modal birefringence or to control the polarization degeneration of the light wave for important communi-

cations and sensor applications. The powerful finite element method can be used to represent such a complex structure accurately, and this work has shown that this approach is also versatile and effective especially when combined with other physical models, such as the acousto-optic, thermo-optic, elasto-optic, and electro-optic models. As a result, it is extremely useful to optimize various novel PCF based components for future applications in communications and sensing in particular.

REFERENCES

1 J.C. Knight, T.A. Birks, P.S.J. Russell, D.M. Atkin, Opt. Lett. **21**, 1547 (1996)
2 T.A. Birks, J.C. Knight, P.S.J. Russell, Opt. Lett. **22**, 961 (1997)
3 J.K. Ranka, R.S. Windeler, A.J. Stentz, Opt. Lett. **25**, 25 (2000)
4 K. Tajima, Y. Sasaki, J. Lightwave Technol. **7**, 674 (1989)
5 Y. Liu, B.M.A. Rahman, K.T.V. Grattan, Appl. Opt. **33**, 5611 (1994)
6 A. Ortigosa-Blanch, J.C. Knight, W.J. Wadsworth, J. Arriaga, B.J. Mangan, T.A. Birks, P.S.J. Russell, Opt. Lett. **25**, 1325 (2000)
7 J. Ju, W. Jin, M.S. Demokan, IEEE Photon. Technol. Lett. **15**, 1375 (2003)
8 K. Suzuki, H. Kubota, S. Kawanishi, M. Tanaka, M. Fujita, Opt. Express **9**, 676 (2001)
9 M.J. Steel, R.M. Osgood, J. Lightwave Technol. **19**, 495 (2001)
10 T.L. Wu, C.-H. Chao, IEEE Photon. Technol. Lett. **16**, 126 (2004)
11 T.P. Hansen, J. Broeng, S.E.B. Libori, E. Knudsen, A. Bjarklev, J.R. Jensen, H. Simonsen, IEEE Photon. Technol. Lett. **13**, 588 (2001)
12 F.C. McNeillie, E. Riis, J. Broeng, J.R. Folkenberg, A. Petersson, H. Simsonsen, C. Jacobsen, Opt. Express **12**, 3981 (2004)
13 G. Kakarantzas, A. Ortigosa-Blanch, T.A. Birks, P.S.J. Russell, L. Farr, F. County, B.J. Mangan, Opt. Lett. **28**, 158 (2003)
14 J. Ju, W. Jin, M.S. Demokan, IEEE Photon. Technol. Lett. **16**, 2472 (2004)
15 J. Broeng, S.E. Barkou, T. Sondergaard, A. Bjarklev, Opt. Lett. **25**, 96 (2000)
16 A. Ferrando, E. Silvestre, J.J. Miret, P. Andres, M.V. Andres, Opt. Lett. **24**, 276 (1999)
17 D. Mogilevtsev, T.A. Birks, P.S.J. Russell, Opt. Lett. **23**, 1662 (1998)
18 T.M. Monro, D.J. Richardson, N.G.R. Broderick, P.J. Bennett, J. Lightwave Technol. **17**, 1093 (1999)
19 B.J. Eggleton, P.S. Westbrook, C.A. White, C. Kerbage, R.S. Windeler, G.L. Burdge, J. Lightwave Technol. **18**, 1084 (2000)
20 T.M. Monro, P.J. Bennett, N.G.R. Broderick, D.J. Richardson, Opt. Lett. **25**, 206 (2000)
21 T.P. White, R.C. McPhedran, C.M. de Sterke, L.C. Botten, M.J. Steel, Opt. Lett. **26**, 1660 (2001)
22 W. Zhi, G.B. Ren, S.Q. Lou, J. Lightwave Technol. **22**, 903 (2004)
23 V. Finazzi, T.M. Monro, D.J. Richardson, Proc. Opt. Fiber Commun. Conf., 524 ThS4, Anaheim, CA (2002)
24 R. Ghosh, A. Kumar, J.P. Meunier, E. Marin, Opt. Quantum Electron. **32**, 963 (2000)
25 F. Fogli, L. Saccomandi, P. Bassi, G. Bellanca, S. Trillo, Opt. Express **10**, 54 (2002)
26 K. Saitoh, M. Koshiba, IEEE J. Quantum Electron. **QE-38**, 927 (2002)
27 Y.Z. He, F.G. Shi, Opt. Commun. **225**, 151 (2003)
28 S.S.A. Obayya, B.M.A. Rahman, K.T.V. Grattan, IEEE Proc. J. Optoelectron. **152**, 241 (2005)
29 B.M.A. Rahman, J.B. Davies, J. Lightwave Technol. **2**, 682 (1984)
30 M. Koshiba, K. Saitoh, Appl. Opt. **42**, 6267 (2003)
31 F. Brechet, J. Marcou, D. Pagnoux, P. Roy, Opt. Fiber Technol. **6**, 181 (2000)
32 A. Peyrilloux, T. Chartier, A. Hideur, L. Berthelot, G. Melin, S. Lempereur, D. Pagnoux, P. Roy, J. Lightwave Technol. **21**, 536 (2003)
33 A. Cucinotta, S. Selleri, L. Vincetti, M. Zoboli, IEEE Photon. Technol. Lett. **14**, 1530 (2002)
34 C. Themistos, B.M.A. Rahman, K.T.V. Grattan, Appl. Opt. **34**, 7695 (1995)
35 A. Cucinotta, F. Poli, S. Selleri, L. Vincetti, M. Zoboli, J. Lightwave Technol. **21**, 782 (2003)
36 K. Saithoh, M. Koshiba, IEEE Photon. Technol. Lett. **15**, 1384 (2003)
37 G.P. Agrawal, *Nonlinear Fibre Optics* 3rd Ed. (Academic Press, London, 2001)
38 J.C. Baggett, T.M. Monro, K. Furusawa, D.J. Richradson, Opt. Lett. **26**, 1045 (2001)
39 S.G. Leon-Saval, T.A. Birks, W.J. Wadsworth, P.S.J. Russell, M.W. Mason, Opt. Express **12**, 2864 (2004)
40 M.A. Foster, A.L. Gaeta, Opt. Express **12**, 3137 (2004)
41 K.P. Hansen, A. Petersson, J.R. Folkenberg, M. Albertsen, A. Bjarklev, Opt. Lett. **29**, 14 (2004)
42 C. Palavicini, Y. Jaouen, G. Debarge, E. Kerrinckx, Y. Quiquempois, M. Douay, C. Lepers, A.-F. Obaton, G. Melin, Opt. Lett. **30**, 361 (2005)
43 B.J. Eggleton, P.S. Westbrook, R.S. Windeler, S. Spalter, T.A. Strasser, Opt. Lett. **24**, 1460 (1999)
44 M. Koshiba, K. Saitoh, IEEE Photon. Technol. Lett. **13**, 1313 (2001)
45 I.-K. Hwang, Y.-J. Lee, Y.-H. Lee, Opt. Express **11**, 2799 (2003)
46 H. Kubota, S. Kawanishi, S. Koyanagi, M. Tanaka, S. Yamaguchi, IEEE Photon. Technol. Lett. **16**, 182 (2004)
47 J.R. Folkenberg, M.D. Nielsen, C. Jackobsen, Opt. Lett. **30**, 1446 (2005)
48 J.R. Folkenberg, M.D. Nelsen, N.A. Mortensen, C. Jackobsen, H.R. Simonsen, Opt. Express **12**, 956 (2004)
49 C. Kerbage, P. Steinvurzel, P. Reyes, P.S. Westbrook, R.S. Windeler, A. Hale, B.J. Eggleton, Opt. Lett. **27**, 842 (2002)
50 Z. Zhu, T.G. Brown, Opt. Lett. **28**, 2306 (2003)